HHS Public Access

Author manuscript

Circ Res. Author manuscript; available in PMC 2023 October 28.

Published in final edited form as:

Circ Res. 2022 October 28; 131(10): e135–e150. doi:10.1161/CIRCRESAHA.122.321384.

Intrapericardial Exosome Therapy Dampens Cardiac Injury Via Activating Foxo3

Dashuai Zhu[1,2,†], **Shuo Liu**[1,2,†], **Ke Huang**[1,2,†], **Zhenzhen Wang**[1,2], **Shiqi Hu**[1,2], **Junlang Li**[1,2], **Zhenhua Li**[1,2], **Ke Cheng**[1,2,*]

[1]Department of Molecular Biomedical Sciences, North Carolina State University, Raleigh, NC 27606, USA

[2]Joint Department of Biomedical Engineering, University of North Carolina at Chapel Hill & North Carolina State University, Raleigh, NC 27606, USA

Abstract

Background: Mesenchymal stem cell (MSC)-derived exosomes are well recognized immunomodulating agents for cardiac repair, while the detailed mechanisms remain elusive. The pericardial drainage pathway provides the heart with immunosurveillance and establishes a simplified model for studying the mechanisms underlying the immunomodulating effects of therapeutic exosomes.

Methods: Myocardial infarction (MI) models with and without pericardiectomy (corresponding to Tomy MI and NonTomy MI) were established to study the functions of pericardial drainage pathway in immune activation in cardiac-draining mediastinal lymph node (MLN). Using the NonTomy MI model, MSC exosomes or vehicle PBS was intrapericardially injected for MI treatment. Via cell sorting and RNA-sequencing (RNA-seq) analysis, the differentially expressed genes were acquired for integrated pathway analysis to identify responsible mechansims. Further through functional knockdown/inhibition studies, application of cytokines and neutralizing antibodies, western blot, flow cytometry and cytokine array, the molecular mechanisms were studied. In addition, the therapeutic efficacy of intrapericardially injected exosomes for MI treatment was evaluated through functional and histological analyses.

Results: We show that the pericardial draining pathway promoted immune activation in the MLN following MI. Intrapericardially injected exosomes accumulated in the MLN and induced regulatory T cell differentiation to promote cardiac repair. Mechanistcally, uptake of exosomes by major histocompatibility complex (MHC)-II$^+$ antigen-presenting cells (APCs) induced forkhead box O3 (Foxo3) activation via the protein phosphatase (PP)-2A/p-Akt/Foxo3 pathway. Foxo3 dominated APC cytokines (IL-10, IL-33, IL-34) expression and built up a Treg-inducing niche in the MLN. The differentiation of Tregs as well as their cardiac deployment were elevated, which contributed to cardiac inflammation resolution and cardiac repair.

[*]**Address for Correspondence:** Ke Cheng, PhD, Dept. of Molecular Biomedical Sciences, NC State University, Dept. of Biomedical Engineering, UNC-Chapel Hill & NC State University, Division of Pharmacoengineering and Molecular Pharmaceutics, UNC-Chapel Hill, 1001 William Moore Drive, Raleigh, NC 27607, United States, Tel: 919-513-6157, Fax: 919-513-7301, ke_cheng@ncsu.edu.
[†]Contributed equally

Disclosures: The authors declare no competing interests.

Conclusions: This study reveals a novel mechanism underlying the immunomodulation effects of MSC-exosomes and provides a promising candidate (PP2A/p-Akt/Foxo3 signaling pathway) with a preferred delivery route (intrapericardial injection) for cardiac repair.

Keywords

exosomes; immunomodulation; mesenchymal stem cell; myocardial infaction; regulatory T cell

Subject Terms

Animal Models of Human Disease; Basic Science Research; Cell therapy; Inflammation; Mechanisms

Introduction

Myocardial infarction (MI) is one of the leading causes of death worldwide[1]. After MI, blood-borne leukocytes infiltrate the necrotic myocardium and release various kinds of inflammatory cytokines causing myocardial inflammation[2, 3]. On the one hand, post-MI inflammation promotes necrotic debris clearance and accelerates reparative progress[4]. On the other hand, post-MI inflammation amplifies cardiac injury and deteriorates cardiac function[2], meanwhile contributes to adverse remodeling and heart failure[3, 5]. Anti-inflammatory therapy has been cardioprotective by salvaging cardiomyocytes and reducing infarct size[6, 7]. Of note, mesenchymal stem cell (MSC) and MSC-exosomes are well recognized immunomodulation agents that promote cardiac inflammation resolution and cardiac repair[8-10]. Previous studies employing intravenous (IV), intracoronary (IC) and intramyocardial (IM) injection of MSC-exosomes showed the immunomodulating effects on proinflammatory cytokines secretion[11, 12], macrophage polarization[13], in particularly the induction of Tregs[9, 14-16], which are intrinsic immunosuppressive cells that dampen excessive immune response and benefit to cardiac recovery[17]. However, the detailed mechanisms underlying the induction of Tregs by MSC-exosomes remain elusive.

iPC injection is a novel approach that takes the pericardial cavity as the target for therapeutics infusion[18]. iPC injection has multiple advantages over the IV, IC and IM injections in terms of the feasibility, cost, invasiveness, and therapeutics retention[18]. Even though IV and IC injection can be easily performed, there is ultra-low retention of therapeutics to the heart[18]. Direct IM injection and application of cardiac patch will increase retention of therapeutics in the heart[19]. However, these methods require a complicated NOGA system or open chest surgery that are expensive and invasive. In contrast, iPC injection can be implemented via a minimally invasive procedure solely by using an introducing catheter and yet yield prolonged retention and myocardial distribution of therapeutics[18, 20, 21]. Additionally, pericardial cavity contains pericardial fluid and immune cells that monitor cardiac homeostasis and migrate to MLN in reaction to cardiac injuries[22, 23]. Given the cascades of innate and adaptive immune activation happening in the pericardial draining pathway, we postulate that the pericardial draining trajectory would serve as a simplified and more straightforward model to study the mechanisms underlying the immunomodulating effects of therapeutic agents.

We hypothesize that iPC injection of MSC-exosomes promotes cardiac repair via modulating adaptive immune activation in the cardiac-draining MLN. Rat model of MI was established with preserved pericardium (NonTomy MI), followed by iPC injection of MSC-exosomes. We found that the exosomes were taken up by MHC-II$^+$ antigen-presenting cells (APCs). By sorting MHC-II$^+$ APCs for RNA-seq analysis, the data revealed increased dephosphorylation of transcription factor Foxo3, which ignites the transcription of interleukin (IL)-10, IL-33, IL-34 and builds up a Treg-inducing niche in the MLN. Consequently, the ratio of Tregs in MLN as well as their myocardial deployment were significantly increased. Tregs coordinate inflammation resolution and cardiac repair by inducing neutrophils apoptosis and macrophage polarization. Cardiac function and histology were improved at a long term follow up. Taken together, this study revealed key functions of Foxo3 underlies the Treg induction by MSC-exosomes for cardiac repair.

Methods

Data Availability

Detailed Materials and Methods are available in the Supplemental Materials. Additional data, analytical methods and materials supporting the conclusions of the study will be available from the corresponding author with reasonable request.

Animals

All animal studies complied with the ethical regulations of NC State University, under the approval of IACUC at NC State University (Protocol#19-811-B). Male Sprague-Dawley (SD) rats, strain code 400, at 8-weeks of age, were used in this study. Rats were housed with 12h light/12h dark cycle at the temperature of 25 °C with 40–60% humidity. Please see the Major Resources Table in the Supplemental Materials.

MSC culture, exosome isolation and characterization

Human umbilical cord derived MSCs were purchased from the American Type Culture Collection (ATCC, VA, USA)[24]. After four passages, serum-free Iscove's modified Dulbecco's medium (IMDM) was changed for conditioned medium collection. The conditioned medium was filtrated through a 0.22μm filter, followed by exosomes isolation using the KrosFlo® KR2i Tangential Flow Filtration (TFF) System (Repligen, United States). Exosome size was characterized by Nanosight[25, 26]; protein concentration and expression of miR-21-5p were measured to indicate the consistency of exosome contents. To trace the distribution of exosomes, DiD (10μM) was added to incubate exosomes at room temperature (RT) for 30 min.

Rat MI model and iPC injection

NonTomy MI models were established by ligating pericardium together with the left anterior descending artery (LAD). Briefly, rats were anesthetized via isoflurane inhalation (2% in oxygen), followed by intubation, thoracotomy, and heart exposure. The LAD was ligated using 6-0 suture. A Hamilton gastight syringe equipped with a 22G needle was used for iPC injection, the volume is 100 μL. To establish Tomy-MI model, bilateral pericardium was removed via pericardiectomy, followed by LAD ligation. The chest wall was closed, the

rats were allowed to recovery. After surgery, the rats were given continuous 3 injections of buprenex (0.01mg/kg) and carpofen (5mg/kg) intraperitoneally for pain management. The models with obvious pale color change in the cardiac apex were randomly deployed to groups and received corresponding treatment. No animals were excluded from the study.

To visualize the pericardial fluid drainage pathway, rats were anesthetized by 2% isoflurane inhalation. Then the heart was exposed. Methylene blue (10mg/mL, 100μL) was injected to the pericardial cavity. The rats were sedated and ventilated for 1 hour. Then the distribution of the blue dye was observed.

Cytokines and neutralizing antibodies

The neutralizing antibody of anti-CD25 (OX-39, Ab00552-1.1) was purchased from the Absolute Antibody company. Anti-CD25 antibody (100μg) was intrapericardially injected to deplete Tregs. To study the functions of IL-10, IL-33 and IL-34, the cytokines and the corresponding neutralizing antibodies were iPC injected with a dose of 2μg and 100μg respectively.

Flow cytometry

At indicated time points, the MLN was collected and macerated through a 40 μm strainer to prepare single cell suspension. After lysis of red blood cells, the cell pellet was resuspended and used for antibody incubation. The antibody information was listed in Supplementary Table 2. After staining, the cells were fixed with 1 % PFA and the samples were analyzed using the Becton Dickinson LSRII flow cytometer (BD Bioscience). Fluorescence-activated cell sorting (FACS) was performed immediately after staining, by using Beckman Coulter MoFlo XDP. Flow cytometry analysis and FACS were accomplished in the Flow Cytometry and Cell Sorting Facility at the College of Veterinary Medicine of NC State University.

RNA-seq and qRT-PCR

The RNA samples (n=3 for each group) extracted from cells of fluorescence-activated cell sorting were used for RNA-seq. To proceed with qRT-PCR, total RNA was extracted using TRIzol reagent (Invitrogen, 15596026). After quantification, 1 μg total RNA template was used for cDNA synthesis using iScript cDNA Synthesis Kit (Bio-Rad, 1708891). qRT-PCR was performed with SsoAdvanced Universal SYBR Green Supermix (Bio-Rad, 1725271). The relative expression was calculated by comparative Ct method. The primer sequences can be acquired in Supplementary Table 1.

Cytokine array

Rat cytokine array was performed by using commercially available kit (Rat cytokine array panel A, R&D systems). The MLN was collected and homogenized in PBS supplemented with protease inhibitor (1mM PMSF). After homogenization, Triton X-100 was added to a final concentration of 1%. Then the samples were store at −80°C. After thaw and centrifuge at 10000g for 5 min, the supernatant was collected for cytokines detection.

Western blot

The samples were lysed in RIPA buffer supplemented with proteinase inhibitor (0.1mM PMSF, ThermoFisher, Catalog#36978), followed by protein extraction and quantification via BCA assay (ThermoFisher, Catalog#23225). After denaturing and separation on Mini-PROTEAN TGX Stain-Free Precast Gels (Bio-Rad), the samples were transferred to PVDF membranes, which was blocked with 5% milk in TBST (w/v) at room temperature (RT) for 1 hour, followed by primary antibodies incubation at 4 °C on a shaking platform. After three washes, the membranes were incubated with horseradish peroxidase-conjugated secondary antibodies for 1 hour at RT. Then the enhanced chemiluminescence (ECL) kit (Bio-Rad, catalog#1705061) was used for colorization and images were acquired using ChemiDoc Imaging System (Bio-Rad).

Measurement of cardiac function

Transthoracic echocardiograph was performed by using Phillips CX30 equipped with a 15MHz probe. The rat was anesthetized with inhalation of 2% isoflurane mixed with oxygen. B-mode image was first acquired, followed by long-axis M-mode imaging, left ventricular (LV) internal diameter at the end diastole (LVIDd) and systole (LVIDs), LV volume at end-diastole (LV-EDV), end-systole (LV-ESV), and LV ejection fraction (LV-EF) were measured. All measurements were acquired from three continuous cardiac cycles.

Histological analysis

At indicated time points, rats were anesthetized by intraperitoneal injection of Ketamin-Xylazine. Following intracardiac perfusion of chilled PBS, the heart and MLN were collected and fixed with 10% NBF for 24 hours. After washing with PBS for 2 hours, the tissues were transferred to 30% (w/v) sucrose and incubated for 24 hours before embedding with OCT compound. A series of cryosections, 5μm-in-thickness, were cut and stored at −20°C for use.

Trichrome Masson staining was performed by following the user manual using commercial kit (Sigma, HT15-1KT). Picrosirius red staining was performed according to the manual (Abcam, ab150681). To perform immunostaining, cryosections were washed with PBS and balanced with blocking serum at RT for 1 hour, followed by incubation of primary antibodies at 4°C overnight. After three washes with PBS, the corresponding secondary antibodies were added for incubation at RT for 2 hours. DAPI-containing Fluoromount-G (Southern Biotech, 0100-20) was used for nucleus staining. TUNEL staining was performed by referring to the user manual (Promega, G3250). The antibodies used in this study were listed in Supplementary Table 2. Imaging was performed using the Olympus FLUOVIEW FV3000 confocal laser scanning microscope or ECHO Revolve microscope.

Statistical analysis

Data acquisition and analysis were performed by investigators blind to the groups. Images with quantitative values closest to the mean values were selected as representatives. Statistical analysis was performed using GraphPad Prism software (Version 9.4.1), and only within-test corrections were made. Data are expressed as mean ± SD. Normal distribution was evaluated by Shapiro-Wilk test (when sample size (n) ≥ 6). For normally distributed

datasets, unpaired 2-tailed Student *t*-test (two groups) or one-way ANOVA (three or more groups) with Tukey's correction was performed. For data with a small sample size (n<6), nonparametric test was applied. Comparison between two groups (both single and multiple comparisons for data acquired from different time points in Fig.1G, Fig. 3H, I) was performed using unpaired 2-tailed nonparametric Mann-Whitney test. Comparison for more than two groups was performed using Kruskal-Wallis's test with Dunn's correction. As for data with two or more subcategories (Fig. 3G), two-way ANOVA with Tukey's correction was performed. $p<0.05$ was accepted as significant difference.

Results

Pericardial fluid drainage into mediastinal lymph node

Pericardial fluid drainage into lymphatic circulation provides critical immunosurveillance for cardiac homeostasis[22]. To clearly show the pericardial draining trajectory, we injected a blue dye into the pericardial cavity (Fig. S1). After 1h drainage, the diffusion of blue dye into the cardiac-draining MLN was observed (Fig. S1). The afferent lymph vessels that are organized in the pericardium aided in the fluid transition (Fig. S1). With this method, we clearly showed the pericardial drainage trajectory.

Pericardial drainage accelerates immune activation in MLN following MI

During the establishment of MI model, pericardiectomy is commonly performed to visualize LAD. To investigate the influence of pericardiectomy on immune activation in the MLN, we introduced NonTomy-MI model, in which the LAD ligation was performed without pericardiectomy (Fig. 1A). The responses in MLN were compared to Tomy-MI models that were established following pericardiectomy (Fig. 1A). The MLN of NonTomy rats enlarged rapidly following MI (Fig. 1B), accompanied with significantly increased cell counts (Fig. 1C, Fig. S2A). Next by detecting MHC-II expression, we found that the $CD45^+MHC\text{-}II^+$ APCs were significantly increased in the MLN of NonTomy rats compared to Tomy rats (Fig. 1D, E, Fig. S2B, C). Upon the migration of APCs into the lymph node, the proliferating cells were robustly elevated in NonTomy-MI rats (Day 1-2, Fig. 1F-H). Flow cytometric analysis indicated increased $CD4^+$ T cells proliferation in the MLN of NonTomy MI rats (Fig. S2D, E and Fig. S3), which benefit to necrotic clearance[27]. The ratio of $ki67^+$ proliferating cells in NonTomy rats was decreased at day 3 (Fig. 1F-H), suggesting regional amelioration of acute myocardial inflammation. However, the proliferation ratio in Tomy-MI rats had persistent increase (Fig. 1F, G), showing features of chronic inflammation that is associated with adverse remodeling[4, 28]. In addition, histological analysis showed protective roles of pericardium in MI hearts (Fig. S4). In normal rats (without LAD ligation), removal of pericardium caused epicardial hyperplasia, accompanied by inflammatory infiltration in both the epicardial and myocardial layers (Fig. S4A). Under the setting of MI, pericardiectomy resulted in persistent cardiac edema (Fig. S4B) and necrotic stacks (Fig. S4C), suggesting compromised clearance of debris that contributes to chronic inflammation.

Next, we sorted $MHC\text{-}II^+$ cells from transgenic GFP rats and injected them into the pericardial cavity of wild type rats with MI injury. The distribution of $GFP^+MHC\text{-}II^+$ cells in the MLN of wild type rats was detected (Fig. S5). The results indicated that pericardial

drainage trajectory served as a direct path for APCs migration towards the cardiac-draining MLN. To investigate whether APC migration towards MLN would lead to improvement in cardiac remodeling, we intrapericardially injected CCR7 inhibitor (cmp2105) to block APC trafficking. The number of $CD45^{+}MHC\text{-}II^{+}$ APCs in MLN and the cardiac histology after 4-week follow up were analyzed (Fig. S6). These results showed that a high dose of CCR7 inhibitor effectively abolished the migration of $CD45^{+}MHC\text{-}II^{+}$ APCs into the MLN (Fig. S6A, B), following which the Treg ratios in the MLN were reduced (Fig. S6C). In addition, CCR7 inhibition exacerbated cardiac remodeling as shown by increased infarct size (Fig. S6D), decreased scar thickness (Fig. S6E), and reduced values of left ventricular ejection fraction (LV-EF) and fractional shortening (LV-FS) (Fig. S6F, G), suggesting that blocking APC trafficking to MLN decreased Treg generation and worsened cardiac remodeling. Taken overall, the above data elucidated the protective roles of pericardial drainage trajectory in promoting adaptive immune activation after MI. These data also make the pericardial drainage trajectory a simplified model for investigating the immunomodulation effects of therapeutics following cardiac injury.

iPC injection of MSC-exosomes for MI treatment

We employed NonTomy MI models to explore the mechanisms underlying the immunomodulation effects of MSC-exosomes. Characterization of exosomes acquired from different batches revealed consistency (Fig. S7). After establishing NonTomy-MI models, MSC-exosomes were intrapericardially injected (iPC-Exo) (Fig. 2A). Control rats received sterile PBS (iPC-PBS) (Fig. 2A). DiD labelling was performed to trace the distribution of exosomes. The enrichment of exosomes into the MLN was observed under a stereo fluorescent microscope (Fig. 2B). Immunofluorescence staining indicated epicardial and pericardial uptake of exosomes after intrapericardial injection (Fig. S8). However, due to the efficient drainage of pericardial fluid into the MLN[22], lymphatic circulation would be the primary pathway of exosomes diffusion (Fig. 2B). Flow cytometry analysis revealed that the injected exosomes were majorly taken up by $MHC\text{-}II^{+}$ cells (Fig. 2Cand Fig. S9). These results implied that the immunomodulating effects of MSC-exosomes are intermediated by $MHC\text{-}II^{+}$ APCs.

Uptake of exosomes promotes Foxo3 activation in APCs

We sorted $MHC\text{-}II^{+}$ APCs for RNA-seq analysis (Fig. 2D) and identified 2336 differentially expressed genes (1227 upregulated genes and 1109 downregulated genes). Through KEGG pathway enrichment and pathway integration analysis (Fig. 2E, F), we found that these pathways confluent on the transcription factor Foxo3 (Fig. 2F). The expression of Foxo3 in APCs was increased after MSC exosome treatment (Fig. 2G). Intracellular activities of Foxo3 are determined by phosphorylation and dephosphorylation modifications[29]. Protein kinase B (Akt) is a key upstream modulator that inhibits the transcriptional activities of Foxo3 by Ser^{253} phosphorylation[29]. In reverse, protein phosphatase 2 (PP2A) counteracts as kinase inhibitor quenches target protein phosphorylation by Akt[30]. The mRNA level of *Ppp2ca* (PP2A) was increased after MSC exosome treatment (Fig. 2G). To gain insights into the protein levels, western-blot was performed to detect PP2A, p-Akt, total Akt as well as the phosphorylation status of Foxo3 (Fig. 2H, Fig. S10). The protein levels of PP2A and Foxo3 were increased after MSC-exosomes treatment, companied with decreased

volume of p-Akt and Foxo3-p253 (p-Foxo3) (Fig. 2H, Fig. S10). Application of LB-100 (a PP2A inhibitor) abolished the effects of MSC-exosomes on Foxo3 dephosphorylation (Fig. 2H, Fig. S10). These results suggested that PP2A could be a critical upstream effector to activate Foxo3. Next, we confirmed the expression of Foxo3 in APCs by flow cytometry (Fig. S11A-C). Foxo3$^+$ cell counts in mediastinal lymph node were increased after exosomes treatment (Fig. S11B), MHC-II$^+$ cells constituted >80% of Foxo3$^+$ cells (Fig. S11C). DiD-labeled exosome colocalized with Foxo3$^+$ cells (Fig. S11D). Furthermore, immunofluorescent staining revealed increased Foxo3 expression in APCs after exosome treatment; however, the level of Foxo3-p253 was significantly decreased in iPC-Exo group (Fig. 2I, Fig. S11E). Taken together, above results suggested that MSC-exosomes treatment promoted Foxo3 activation in APCs.

Foxo3 dominates APC cytokine expression to establish Treg-inducing niche

To figure out the downstream target genes of Foxo3, we performed online prediction by using CHEA and TRSNSFAC datasets[31](Fig. 3A). Of note, the predicted genes involve major histocompatibility complex (MHC-I, MHC-II), costimulatory molecules (SLAM6, TNFSF8, TNFSF18) as well as a series of cytokines (IL-10, IL-15, IL-33, IL-34) (Fig. 3A). All of these molecules are implicated in antigen specific T cell priming and activation, especially the released cytokines can direct the differentiation of effector T cells into specific subtypes[32]. We next acquired the DNA binding motif of Foxo3 from online database JASPAR (Fig. 3B) and analyzed the potential binding sites of Foxo3 in the promoter sequence of above cytokine genes (Fig. 3C). Analysis of cytokines expression from RNA-seq data indicated increased IL-10, IL-33 and IL-34 levels in MSC-exosomes treated APCs (Fig. S12A). These results showed that Foxo3 could serve as a potent transcription factor for starting the expression of IL-10, IL-33 and IL-34, which have been reported to induce Treg differentiation[33-36].

Therefore, we performed loss-of-function studies to investigate the roles of Foxo3 in IL-10, IL-33, and IL-34 expression. Firstly, we confirmed that Foxo3 is necessary for inducing IL-10, IL-33, and IL-34 expression in APCs. Knockdown of Foxo3 by siRNA resulted in decreased IL-10, IL-33, and IL-34 expression in MHC-II$^+$ cells (treated with infarct lysate and exosomes) (Fig. 3D-F). Moreover, intrapericardial injection of PP2A inhibitor LB100 abolished the induction of IL-10, IL-33, and IL-34 expressions by exosomes in APCs (Fig. 3G). These results indicated that Foxo3 is a potent upstream regulator of IL-10, IL-33, and IL-34. Afterwards, we investigated the functions of IL-10, IL-33, and IL-34 in inducing Treg cell differentiation. The number of CD4$^+$Foxp3$^+$ Treg cells in the MLN increased with iPC-Exo treatment (Fig. 3H, I). Intrapericardial injection of neutralizing antibodies targeting IL-10, IL-33 and IL-34 abolished the increase of Treg cells caused by exosomes injection (Fig. 3 J, K). Whereas infusion of the indicated cytokines significantly elevated Treg counts in the MLN of iPC-PBS treated rats (Fig. 3L). Taken together, these results showed that Foxo3 played a critical role in Treg induction by upregulating IL-10, IL-33, and IL-34 expression.

We next performed cytokine array using the tissue lysates made from the whole MLN (Fig. S12B-D). The quantitative data showed obvious change in the cytokine profiles of APCs, in

which the volume of Treg-specific IL-10 was increased, whereas the levels of Th1-specific IFN-γ and Th17-specific IL-17 were decreased (Fig. S12B-D). These changes were further confirmed by immunostaining (Fig. S13A-C). In addition, flowcytometric analysis showed decreased ratios of IFN-γ^+ Th1 and IL-17^+ Th17 cells in the MLN of exosomes treated rats (Fig. S13D, E). Taken overall, these results illustrated that activation of Foxo3 in $CD45^+MHC\text{-}II^+$ APCs boosted the Treg-inductive cytokines secretion and established a Treg-inducing niche in the MLN.

$MHC\text{-}II^+$ APCs are a compilation of myeloid cells (macrophages and dendritic cells) and B cells[37]. To analyze which subtype of the cells taking up exosomes contributed to Treg expansion, we performed co-culture studies (Fig. S14). Macrophages ($CD68^+$), dendritic cells ($CD11c^+$), and B cells ($B220^+$) were acquired through magnetic-activated cell sorting (MACS) from the MLN of iPC-Exo treated MI rats, and then the cells were cocultured with $CD4^+$ T cells. Treg differentiation was detected by flow cytometry (Fig. S14A, B). The results showed that $CD11c^+$ dendritic cells had the most robust effect on Treg induction (Fig. S14C, D). However, detection of Foxo3 expression by immunofluorescence staining (Fig. S14E) indicated that Foxo3 could be involved in all three cell types to induce Treg differentiation.

iPC exosome treatment promotes cardiac deployment of Tregs

Following the increased Treg differentiation in the MLN of iPC-Exo treated rats, myocardial deployment of $CD4^+Foxp3^+$ Tregs was increased as detected by immunostaining (Fig. 4A, B) and flowcytometric analysis (Fig. 4C-F). Further by detecting the expression of Treg-specific cytokines (IL-35, IL-33, IL-13, and IL-10) in the myocardium (Fig. 4G), these datasets suggested that iPC injection of MSC-exosomes promoted Tregs differentiation and their myocardial deployment.

To test whether cytokines (IL-10, IL-33, and IL-34) modulation could affect the infiltration of Tregs in the heart, we detected cardiac infiltration of Tregs after cytokine mix or neutralizing antibody cocktail infusion. The results showed that neutralizing IL-10, IL-33, and IL-34 reduced the cardiac infiltration of Tregs, whereas injection of the cytokines increased Treg counts in the heart (Fig. S15).

Tregs orchestrate myocardial inflammation resolution

Neutrophils and monocytes/macrophages are the primary immune cells infiltrate the infarcted myocardium to cause post-MI inflammation[2, 38]. These cells release proinflammatory cytokines to enlarge immune cascades, meanwhile, exacerbate the apoptosis of cardiomyocytes[38, 39]. In contrast, Tregs exert immunosuppressive functions to extinguish the proinflammatory responses of innate immune cells following MI[12]. To investigate the influence of Tregs deployment on cardiac inflammation, we first performed TUNEL assay to detect apoptosis. By using myeloperoxidase (MPO) as a marker of neutrophils, the myocardial infiltration of MPO^+ neutrophils were decreased because of increased apoptosis in iPC-Exo group (Fig. 5A-C), and the apoptotic cardiomyocytes were reduced after exosomes treatment (Fig. 5D). Next, we analyzed macrophage polarization by employing SOCS3 and CD206 as the markers (Fig. 5E-I). Treatment with exosomes

decreased SOCS3$^+$ pro-inflammatory macrophages (Fig. 5E, G), whereas the number of CD206$^+$ pro-reparative macrophages (Fig. 5F, H) and the ratio of CD206$^+$ macrophage in total macrophages (Fig. 5I) were increased. Further by evaluating the expression of macrophage associated cytokines in the infarct (Fig. S16), these data confirmed the inflammation resolution in iPC-Exo treated MI hearts. However, depletion of Tregs using anti-CD25 antibody aggravated cardiac inflammation in iPC-PBS treated rats and abrogated the protective actions of exosomes (Fig. 5A-I, Fig. S17). These results indicated protective roles of Tregs in post-MI inflammation resolution, meanwhile suggested Treg dependent effects of exosomes. Taken together, above results showed that Tregs deployment in the injured myocardium promoted post-MI inflammation resolution.

Improved cardiac repair by iPC injection of exosomes

Beside the myocardial inflammation resolution, there were increased vascular regeneration in MSC-exosomes treated hearts (Fig. S18). TTC staining confirmed the comparable initial infarct area between groups (Fig. S19). To gain insights of long-term outcomes of MI following iPC-Exo treatment, Masson's trichrome staining was performed to measure infarct size (Fig. 6A, B). Exosomes treatment ameliorated cardiac remodeling as indicated by decreased infarct size (Fig. 6B) and increased scar thickness (Fig. 6C). Further by performing picrosirius red staining (Fig. S20), we found that the deposition of type 1 collagen was significantly reduced by exosomes treatment, whereas levels of type 3 collagen were elevated (Fig. 6D, E). Depletion of Tregs expanded infarct size and worsened cardiac remodeling in both iPC-PBS and iPC-Exo treated MI hearts (Fig. 6A-E). Next, we performed echocardiography to analysis cardiac functions (Fig. 6F). The LV-EF was improved by exosomes injection (Fig. 6G), and LV dimensions were well preserved by exosomes treatment (Fig. 6H-K), whereas the LV dimensions of iPC-PBS treated hearts showed obvious enlargement that indicating dilated cardiomyopathy (Fig. 6H-K). Moreover, Treg depletion caused deterioration of cardiac morphology and function, and compromised the therapeutic effects of exosomes (Fig. 6). Taken together, these data further confirmed the Treg dependent effects of exosomes to modulate the immune response for heart repair (Fig. 7).

Discussion

MSC-exosomes have been reported to modulate post-MI inflammation and benefit to cardiac recovery[40-42]. In previous studies, the immunomodulating effects of exosomes were investigated via IM, IC and IV infusion of exosomes[43, 44], and in particularly, the induction of Tregs by MSC-exosomes has drawn lots of interests in treatment of heart diseases[45, 46]. In this study, we used a pericardial draining model and investigated the mechanisms of immunomodulation by MSC-exosomes. Our data showed that iPC injected exosomes are absorbed by MHC-II$^+$ APCs, and induced Foxo3 activation via modulating PP2A/p-Akt/Foxo3 pathway. Foxo3 promoted expression and secretion of IL-10, IL-33, IL-34 by APCs to establish a Treg-inducing niche in the MLN. Following myocardial deployment, Tregs orchestrate inflammation resolution and cardiac reparation.

Pericardial draining trajectory is a simplified model for studying the mechanisms of immunomodulating agents[47, 48]. The drainage of pericardial fluid by MLN established direct immunosurveillance for the heart[22, 26, 48]. Pericardial fluid dissolves cardiomyocyte metabolites that are critical cues for immune response, especially in the setting of myocardial injuries[48]. Previous studies reported that dendritic cells migrate to MLN following MI[23]. In our study, the APCs migration accelerated the activation of adaptive immune responses in the MLN. APCs play critical roles in the activation of specific subtype of T cells, in particular, the cytokines released by APCs direct T cells differentiation[32]. In this study, we found that the activation of Foxo3 following exosomes uptake potently enhanced the expression and secretion of Treg-inducing cytokines by APCs (Fig. 3). Foxo3 is a transcription factor. Its downstream target genes involve major histocompatibility complex, co-stimulatory molecules as well as a series of interleukins. This gene set contains the complicated signal molecules that are needed for T cell activation and implies the potential roles of Foxo3 in dominating T cell activation[32]. The cytokine profiles of APCs were changed to exhibit Treg-inducing characteristics after exosome treatment (Fig. S12A). For example, IL-10, IL-15 and IL-18 drive Treg differentiation[49, 50], CXCL9, CXCL10, and CCL20 have been reported to promote Treg migration[51-53], while the expression of chemokines (CCL3, CCL4, CCL5) associated with Th1, Th17, and $CD8^+$ T cells that exacerbate cardiac injuries[54-56] were downregulated. Consequently, the generation of Treg was elevated. Whereas the cell counts of Th1 and Th17 were decreased, in consistent with decreased levels of IFN-γ and IL-17a. There are also changes in the other cytokines and chemokines that may be involved in the self-modulation of APCs functions[57]. For example, IL-1 was expected to drive inflammatory response, it can also promote the expression of co-stimulation molecules and MHC complex, which are critical for Tregs priming[57]. From these data, we can conclude that Foxo3 activation promoted to establish a Treg-inducing niche in the MLN.

Tregs orchestrate myocardial inflammation resolution[46, 58, 59]. Following induction in the MLN, Tregs migration to the infarct is essential to exert the immunomodulating actions. CXCR4 is a chemokine receptor that directs T cells infiltration into the injured myocardium from lymph node, along with CXCL12 gradients[15]. Previous CT/PET imaging studies have revealed the existence of MLN-heart axis in MI patients[15]. Given that iPC injected exosomes promoted Treg generation in the MLN, it would be reasonable to conclude that CXCR4/CXCL12 axis aided the Tregs migration to the infarct, following which the neutrophils apoptosis and pro-reparative macrophage polarization were promoted, suggesting myocardial inflammation resolution. However, Tregs depletion abolished the immunomodulating effects of iPC-Exo. In consistent with previous studies[17, 60], these data showed that Tregs coordinate post-MI inflammation resolution and cardiac repair.

The detailed mechanisms responsible for PP2A activation by exosomes treatment remain unclear. However, our data confirmed that PP2A is a potent upstream factor for Foxo3 dephosphorylation. RNA-seq data revealed increased PP2A expression in iPC-Exo treated APCs (Fig. 2G). Application of LB-100 (PP2A inhibitor) reduced Foxo3 activation by 82.6% (Fig. 5H, Fig. S10). In addition, online database predicted that Foxo3 could be a transcription factor for PP2A expression (Fig. 3A). These data established an interactive

loop between PP2A and Foxo3, while the detailed interaction mechanisms need to be further studied.

MHC-II$^+$ APCs are a complex group of different cell types including monocytes, macrophages, dendritic cells, and B cells. One limitation of the present study is that the identity of the specific subtype of MHC-II$^+$ APCs taking up exosomes and trafficking to MLN is not fully defined. Given the results from the co-culture (Fig. S14) and CCR7 inhibition studies (Fig. S6), we postulate that dendritic cells and B cells played critical roles in inducing Tregs as well in improving cardiac remodeling after exosomes treatment. After all, this study revealed novel mechanisms underlying the immunomodulation effects of MSC-exosomes to induce Tregs for post-MI repair, in which the activation of Foxo3 in APCs played critical roles (Fig. 7).

Supplementary Material

Refer to Web version on PubMed Central for supplementary material.

Acknowledgements:

The authors thank the Laboratory Animal Resources (LAR), the Central Procedures Lab (CPL) and the Flow Cytometry and Cell Sorting facility at NC State University for their help with this study. The authors also thank Ms. Andrea Wrecker for proofreading the manuscript.

Source of funding:

This study is supported by grants from the National Institutes of Health (HL123920, HL137093, HL144002, HL146153, HL147357, and HL149940, to K.C.) and the American Heart Association (18TPA34230092 and 19EIA34660286 to K.C.; 21CDA855570 to K.H.).

Nonstandard Abbreviations and Acronyms

MSC	Mesenchymal stem cell
MLN	Mediastinal lymph node
iPC	Intrapericardial
Treg	Regulatory T cell
APC	Antigen presenting cell
MI	Myocardial infarction
LAD	Left anterior descending artery
PP2A	Protein phosphatase 2A
LV-EF	left ventricular ejection fraction
LV-FS	left ventricular fractional shortening
LV-EDV	left ventricular volume at end diastole
LV-ESV	left ventricular volume at end systole

LVIDd	Left ventricular internal diameter at end diastole
LVIDs	Left ventricular internal diameter at end systole

Reference

1. Melhem NJ, Chajadine M, Gomez I, Howangyin KY, Bouvet M, Knosp C, et al. Endothelial cell indoleamine 2, 3-dioxygenase 1 alters cardiac function after myocardial infarction through kynurenine. Circulation. 2021;143:566–580 [PubMed: 33272024]
2. Prabhu SD, Frangogiannis NG. The biological basis for cardiac repair after myocardial infarction: From inflammation to fibrosis. Circulation research. 2016;119:91–112 [PubMed: 27340270]
3. Mewton N, Roubille F, Bresson D, Prieur C, Bouleti C, Bochaton T, et al. Effect of colchicine on myocardial injury in acute myocardial infarction. Circulation. 2021;144:859–869 [PubMed: 34420373]
4. Wan E, Yeap XY, Dehn S, Terry R, Novak M, Zhang S, et al. Enhanced efferocytosis of apoptotic cardiomyocytes through myeloid-epithelial-reproductive tyrosine kinase links acute inflammation resolution to cardiac repair after infarction. Circulation research. 2013;113:1004–1012 [PubMed: 23836795]
5. Westman PC, Lipinski MJ, Luger D, Waksman R, Bonow RO, Wu E, et al. Inflammation as a driver of adverse left ventricular remodeling after acute myocardial infarction. Journal of the American College of Cardiology. 2016;67:2050–2060 [PubMed: 27126533]
6. Deftereos S, Giannopoulos G, Angelidis C, Alexopoulos N, Filippatos G, Papoutsidakis N, et al. Anti-inflammatory treatment with colchicine in acute myocardial infarction: A pilot study. Circulation. 2015;132:1395–1403 [PubMed: 26265659]
7. Huang S, Frangogiannis NG. Anti-inflammatory therapies in myocardial infarction: Failures, hopes and challenges. British journal of pharmacology. 2018;175:1377–1400 [PubMed: 29394499]
8. Zhang Z, Tian H, Yang C, Liu J, Zhang H, Wang J, et al. Mesenchymal stem cells promote the resolution of cardiac inflammation after ischemia reperfusion via enhancing efferocytosis of neutrophils. Journal of the American Heart Association. 2020;9:e014397 [PubMed: 32079474]
9. Song T, Eirin A, Zhu X, Zhao Y, Krier JD, Tang H, et al. Mesenchymal stem cell-derived extracellular vesicles induce regulatory t cells to ameliorate chronic kidney injury. Hypertension. 2020;75:1223–1232 [PubMed: 32223383]
10. Vagnozzi RJ, Maillet M, Sargent MA, Khalil H, Johansen AKZ, Schwanekamp JA, et al. An acute immune response underlies the benefit of cardiac stem cell therapy. Nature. 2020;577:405–409 [PubMed: 31775156]
11. Weiss ARR, Dahlke MH. Immunomodulation by mesenchymal stem cells (mscs): Mechanisms of action of living, apoptotic, and dead mscs. Frontiers in immunology. 2019;10:1191 [PubMed: 31214172]
12. Gao F, Chiu SM, Motan DA, Zhang Z, Chen L, Ji HL, et al. Mesenchymal stem cells and immunomodulation: Current status and future prospects. Cell death & disease. 2016;7:e2062 [PubMed: 26794657]
13. Wysoczynski M, Khan A, Bolli R. New paradigms in cell therapy: Repeated dosing, intravenous delivery, immunomodulatory actions, and new cell types. Circulation research. 2018;123:138–158 [PubMed: 29976684]
14. Azevedo RI, Minskaia E, Fernandes-Platzgummer A, Vieira AIS, da Silva CL, Cabral JMS, et al. Mesenchymal stromal cells induce regulatory t cells via epigenetic conversion of human conventional cd4 t cells in vitro. Stem cells. 2020;38:1007–1019 [PubMed: 32352186]
15. Rieckmann M, Delgobo M, Gaal C, Buchner L, Steinau P, Reshef D, et al. Myocardial infarction triggers cardioprotective antigen-specific t helper cell responses. The Journal of clinical investigation. 2019;129:4922–4936 [PubMed: 31408441]
16. Zacchigna S, Martinelli V, Moimas S, Colliva A, Anzini M, Nordio A, et al. Paracrine effect of regulatory t cells promotes cardiomyocyte proliferation during pregnancy and after myocardial infarction. Nature communications. 2018;9:2432

17. Weirather J, Hofmann UD, Beyersdorf N, Ramos GC, Vogel B, Frey A, et al. Foxp3+ cd4+ t cells improve healing after myocardial infarction by modulating monocyte/macrophage differentiation. Circulation research. 2014;115:55–67 [PubMed: 24786398]
18. Zhu D, Li Z, Huang K, Caranasos TG, Rossi JS, Cheng K. Minimally invasive delivery of therapeutic agents by hydrogel injection into the pericardial cavity for cardiac repair. Nature communications. 2021;12:1412
19. Zhu D, Hou J, Qian M, Jin D, Hao T, Pan Y, et al. Nitrate-functionalized patch confers cardioprotection and improves heart repair after myocardial infarction via local nitric oxide delivery. Nature communications. 2021;12:4501
20. Li Z, Zhu D, Hui Q, Bi J, Yu B, Huang Z, et al. Injection of ros-responsive hydrogel loaded with basic fibroblast growth factor into the pericardial cavity for heart repair. Advanced Functional Materials. 2021;31:2004377
21. Li J, Lv Y, Zhu D, Mei X, Huang K, Wang X, et al. Intrapericardial hydrogel injection generates high cell retention and augments therapeutic effects of mesenchymal stem cells in myocardial infarction. Chemical Engineering Journal. 2022;427:131581
22. Vogiatzidis K, Zarogiannis SG, Aidonidis I, Solenov EI, Molyvdas PA, Gourgoulianis KI, et al. Physiology of pericardial fluid production and drainage. Frontiers in physiology. 2015;6:62 [PubMed: 25852564]
23. Van der Borght K, Scott CL, Nindl V, Bouche A, Martens L, Sichien D, et al. Myocardial infarction primes autoreactive t cells through activation of dendritic cells. Cell reports. 2017;18:3005–3017 [PubMed: 28329691]
24. Zhang S, Zhu D, Li Z, Huang K, Hu S, Lutz H, et al. A stem cell-derived ovarian regenerative patch restores ovarian function and rescues fertility in rats with primary ovarian insufficiency. Theranostics. 2021;11:8894–8908 [PubMed: 34522217]
25. Wen Y, Fu Q, Soliwoda A, Zhang S, Zheng M, Mao W, et al. Cell-derived nanovesicles prepared by membrane extrusion are good substitutes for natural extracellular vesicles. Extracellular Vesicle. 2022;1:100004
26. Zhao J, Xu L, Yang D, Tang H, Chen Y, Zhang X, et al. Exosome-driven liquid biopsy for breast cancer: Recent advances in isolation, biomarker identification and detection. Extracellular Vesicle. 2022;1:100006
27. Hofmann U, Beyersdorf N, Weirather J, Podolskaya A, Bauersachs J, Ertl G, et al. Activation of cd4+ t lymphocytes improves wound healing and survival after experimental myocardial infarction in mice. Circulation. 2012;125:1652–1663 [PubMed: 22388323]
28. DeBerge M, Yeap XY, Dehn S, Zhang S, Grigoryeva L, Misener S, et al. Mertk cleavage on resident cardiac macrophages compromises repair after myocardial ischemia reperfusion injury. Circulation research. 2017;121:930–940 [PubMed: 28851810]
29. Brunet A, Bonni A, Zigmond MJ, Lin MZ, Juo P, Hu LS, et al. Akt promotes cell survival by phosphorylating and inhibiting a forkhead transcription factor. Cell. 1999;96:857–868 [PubMed: 10102273]
30. Kuo YC, Huang KY, Yang CH, Yang YS, Lee WY, Chiang CW. Regulation of phosphorylation of thr-308 of akt, cell proliferation, and survival by the b55alpha regulatory subunit targeting of the protein phosphatase 2a holoenzyme to akt. The Journal of biological chemistry. 2008;283:1882–1892 [PubMed: 18042541]
31. Rouillard AD, Gundersen GW, Fernandez NF, Wang Z, Monteiro CD, McDermott MG, et al. The harmonizome: A collection of processed datasets gathered to serve and mine knowledge about genes and proteins. Database : the journal of biological databases and curation. 2016;2016
32. Gutcher I, Becher B. Apc-derived cytokines and t cell polarization in autoimmune inflammation. The Journal of clinical investigation. 2007;117:1119–1127 [PubMed: 17476341]
33. Bezie S, Freuchet A, Serazin C, Salama A, Vimond N, Anegon I, et al. Il-34 actions on foxp3(+) tregs and cd14(+) monocytes control human graft rejection. Frontiers in immunology. 2020;11:1496 [PubMed: 32849510]
34. Bezie S, Picarda E, Ossart J, Tesson L, Usal C, Renaudin K, et al. Il-34 is a treg-specific cytokine and mediates transplant tolerance. The Journal of clinical investigation. 2015;125:3952–3964 [PubMed: 26389674]

35. Pastille E, Wasmer MH, Adamczyk A, Vu VP, Mager LF, Phuong NNT, et al. The il-33/st2 pathway shapes the regulatory t cell phenotype to promote intestinal cancer. Mucosal immunology. 2019;12:990–1003 [PubMed: 31165767]
36. Hsu P, Santner-Nanan B, Hu M, Skarratt K, Lee CH, Stormon M, et al. Il-10 potentiates differentiation of human induced regulatory t cells via stat3 and foxo1. Journal of immunology. 2015;195:3665–3674
37. Kambayashi T, Laufer TM. Atypical mhc class ii-expressing antigen-presenting cells: Can anything replace a dendritic cell? Nature reviews. Immunology. 2014;14:719–730
38. Ong SB, Hernandez-Resendiz S, Crespo-Avilan GE, Mukhametshina RT, Kwek XY, Cabrera-Fuentes HA, et al. Inflammation following acute myocardial infarction: Multiple players, dynamic roles, and novel therapeutic opportunities. Pharmacology & therapeutics. 2018;186:73–87 [PubMed: 29330085]
39. Santos-Zas I, Lemarie J, Tedgui A, Ait-Oufella H. Adaptive immune responses contribute to post-ischemic cardiac remodeling. Frontiers in cardiovascular medicine. 2018;5:198 [PubMed: 30687720]
40. Zhu D, Cheng K. Cardiac cell therapy for heart repair: Should the cells be left out? Cells. 2021;10
41. Chen X, Zhu L, Liu J, Lu Y, Pan L, Xiao J. Greasing wheels of cell-free therapies for cardiovascular diseases: Integrated devices of exosomes/exosome-like nanovectors with bioinspired materials. Extracellular Vesicle. 2022;1:100010
42. Vaka R, Remortel SV, Ly V, Davis DR. Extracellular vesicle therapy for non-ischemic heart failure: A systematic review of preclinical studies. Extracellular Vesicle. 2022;1:100009
43. Popowski KD, López de Juan Abad B, George A, Silkstone D, Belcher E, Chung J, et al. Inhalable exosomes outperform liposomes as mrna and protein drug carriers to the lung. Extracellular Vesicle. 2022;1:100002
44. Hu S, Li Z, Shen D, Zhu D, Huang K, Su T, et al. Exosome-eluting stents for vascular healing after ischaemic injury. Nature biomedical engineering. 2021;5:1174–1188
45. Zhang B, Yeo RWY, Lai RC, Sim EWK, Chin KC, Lim SK. Mesenchymal stromal cell exosome-enhanced regulatory t-cell production through an antigen-presenting cell-mediated pathway. Cytotherapy. 2018;20:687–696 [PubMed: 29622483]
46. Xia N, Lu Y, Gu M, Li N, Liu M, Jiao J, et al. A unique population of regulatory t cells in heart potentiates cardiac protection from myocardial infarction. Circulation. 2020;142:1956–1973 [PubMed: 32985264]
47. Fatehi Hassanabad A, Zarzycki A, Deniset JF, Fedak PW. An overview of human pericardial space and pericardial fluid. Cardiovascular pathology : the official journal of the Society for Cardiovascular Pathology. 2021;53:107346 [PubMed: 34023529]
48. Trindade F, Vitorino R, Leite-Moreira A, Falcao-Pires I. Pericardial fluid: An underrated molecular library of heart conditions and a potential vehicle for cardiac therapy. Basic research in cardiology. 2019;114:10 [PubMed: 30659359]
49. Oertli M, Sundquist M, Hitzler I, Engler DB, Arnold IC, Reuter S, et al. Dc-derived il-18 drives treg differentiation, murine helicobacter pylori-specific immune tolerance, and asthma protection. The Journal of clinical investigation. 2012;122:1082–1096 [PubMed: 22307326]
50. Xia J, Liu W, Hu B, Tian Z, Yang Y. Il-15 promotes regulatory t cell function and protects against diabetes development in nk-depleted nod mice. Clinical immunology. 2010;134:130–139 [PubMed: 19875339]
51. Li CX, Ling CC, Shao Y, Xu A, Li XC, Ng KT, et al. Cxcl10/cxcr3 signaling mobilized-regulatory t cells promote liver tumor recurrence after transplantation. Journal of hepatology. 2016;65:944–952 [PubMed: 27245433]
52. Tokunaga R, Zhang W, Naseem M, Puccini A, Berger MD, Soni S, et al. Cxcl9, cxcl10, cxcl11/cxcr3 axis for immune activation - a target for novel cancer therapy. Cancer treatment reviews. 2018;63:40–47 [PubMed: 29207310]
53. Chen KJ, Lin SZ, Zhou L, Xie HY, Zhou WH, Taki-Eldin A, et al. Selective recruitment of regulatory t cell through ccr6-ccl20 in hepatocellular carcinoma fosters tumor progression and predicts poor prognosis. PloS one. 2011;6:e24671 [PubMed: 21935436]

54. Murooka TT, Rahbar R, Platanias LC, Fish EN. Ccl5-mediated t-cell chemotaxis involves the initiation of mrna translation through mtor/4e-bp1. Blood. 2008;111:4892–4901 [PubMed: 18337562]

55. Santos-Zas I, Lemarie J, Zlatanova I, Cachanado M, Seghezzi JC, Benamer H, et al. Cytotoxic cd8(+) t cells promote granzyme b-dependent adverse post-ischemic cardiac remodeling. Nature communications. 2021;12:1483

56. Castellino F, Huang AY, Altan-Bonnet G, Stoll S, Scheinecker C, Germain RN. Chemokines enhance immunity by guiding naive cd8+ t cells to sites of cd4+ t cell-dendritic cell interaction. Nature. 2006;440:890–895 [PubMed: 16612374]

57. Van Den Eeckhout B, Tavernier J, Gerlo S. Interleukin-1 as innate mediator of t cell immunity. Frontiers in immunology. 2020;11:621931 [PubMed: 33584721]

58. Choo EH, Lee JH, Park EH, Park HE, Jung NC, Kim TH, et al. Infarcted myocardium-primed dendritic cells improve remodeling and cardiac function after myocardial infarction by modulating the regulatory t cell and macrophage polarization. Circulation. 2017;135:1444–1457 [PubMed: 28174192]

59. Jia D, Jiang H, Weng X, Wu J, Bai P, Yang W, et al. Interleukin-35 promotes macrophage survival and improves wound healing after myocardial infarction in mice. Circulation research. 2019;124:1323–1336 [PubMed: 30832557]

60. Wang Y, Dembowsky K, Chevalier E, Stuve P, Korf-Klingebiel M, Lochner M, et al. C-x-c motif chemokine receptor 4 blockade promotes tissue repair after myocardial infarction by enhancing regulatory t cell mobilization and immune-regulatory function. Circulation. 2019;139:1798–1812 [PubMed: 30696265]

Nolvety and Significance

What is Known?

- Mesenchymal stem cell (MSC) derived exosomes promote cardiac repair after myocardial infarction (MI).
- Regulatory T cells (Tregs) orchestrate cardiac inflammation resolution and cardiac repair.
- MSC exosomes suppress post-MI inflammation and improve cardiac remodeling via priming Tregs, while the mechanisms remain elusive.

What New Information Does This Article Contribute?

- The pericardial draining trajectory provides a short-cut route for therapeutic agents that are injected into the pericardial space to impart their immunomodulating effects.
- Intrapericardially (iPC) injected MSC exosomes are taken up by major histocompatibility complex (MHC)-II+ antigen presenting cells (APCs) and activate PP2A/p-Akt/Foxo3 pathway in APCs.
- Foxo3 dominates Treg induction by APCs to promote cardiac repair.

This study used an intrapericardial draining model to dissect the immunomodulating mechanisms underlying the therapeutic benefits of MSC exosomes and revealed critical roles of PP2A/p-Akt/Foxo3 pathway in Tregs induction in MSC exosome-mediated cardiac repair. Targeting Foxo3 in APCs could be an effective strategy to activate immunosuppressive Tregs for heart repair. iPC injection can serve as an effective approach to deliver regenerative therapeutics to the heart.

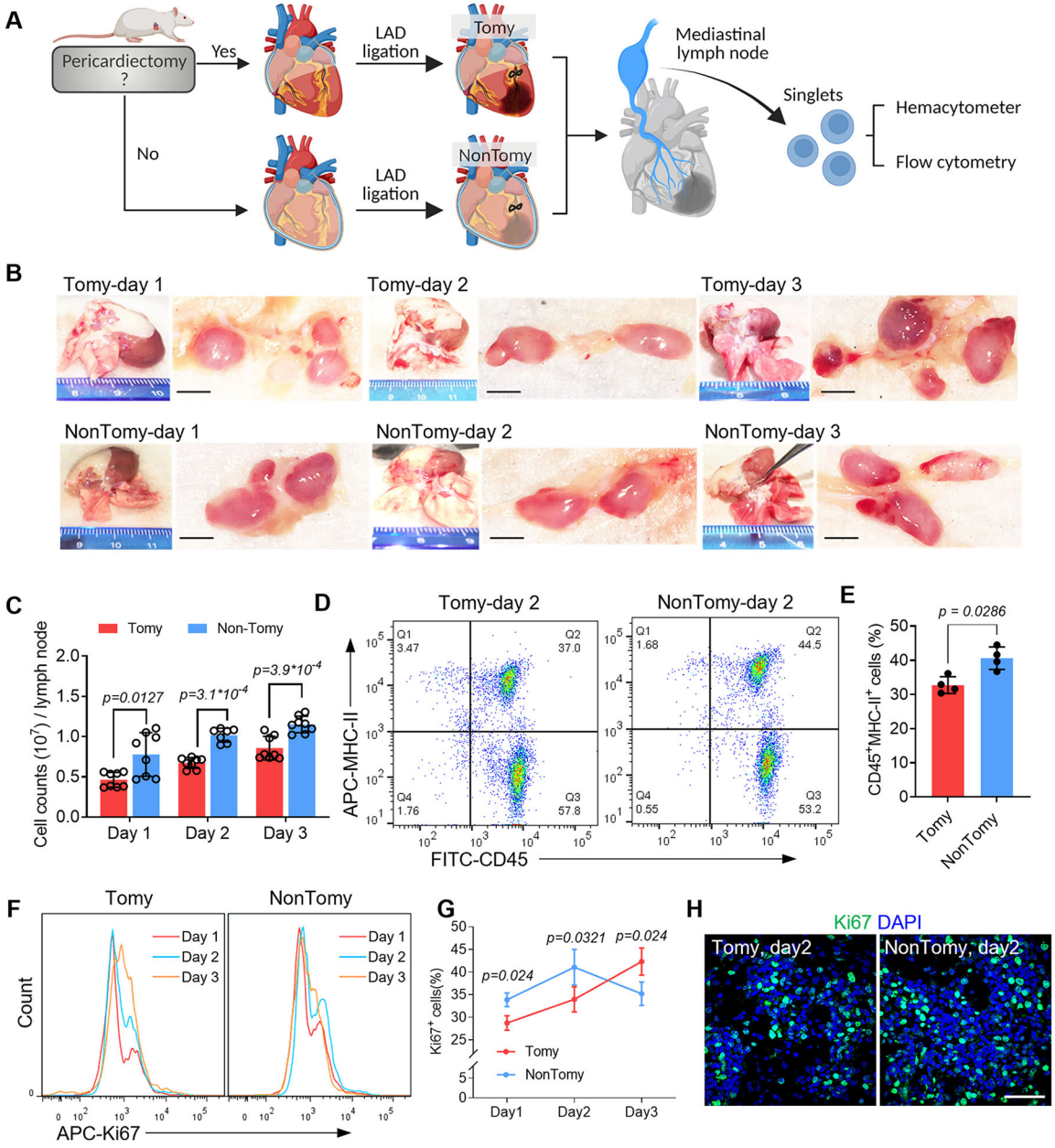

Figure 1. Pericardial drainage promotes immune activation in cardiac-draining mediastinal lymph node (MLN).

(A) Schematic study design. **(B)** Macroscopic examination of the cardiac-draining MLN. Scale bar, 1mm. **(C)** Cell counts in each MLN was measured by using hemacytometer. n=8 lymph nodes for Tomy group (Day 1-3) and NonTomy group (Day 1 and Day 3); n=7 lymph nodes for NonTomy group (Day 2). **(D)** Flow cytometry detection of APC migration in the MLN by using MHC-II as a marker. **(E)** Quantitative data of $CD45^+MHC\text{-}II^+$ cell counts in the MLN. n=4 animals for each group. **(F)** Flow cytometry detection of cell proliferation in the MLN, and accordingly the percentage of $Ki67^+$ cells were plotted **(G)**. n=4 animals for each group. **(H)** Immunofluorescent staining of Ki67 to show the cell proliferation in the MLN. Scale bar, 60μm. Quantitative data was shown as mean ± SD. *p* values were

determined by one-way ANOVA for C; unpaired 2-tailed nonparametric Mann-Whitney test for E, G.

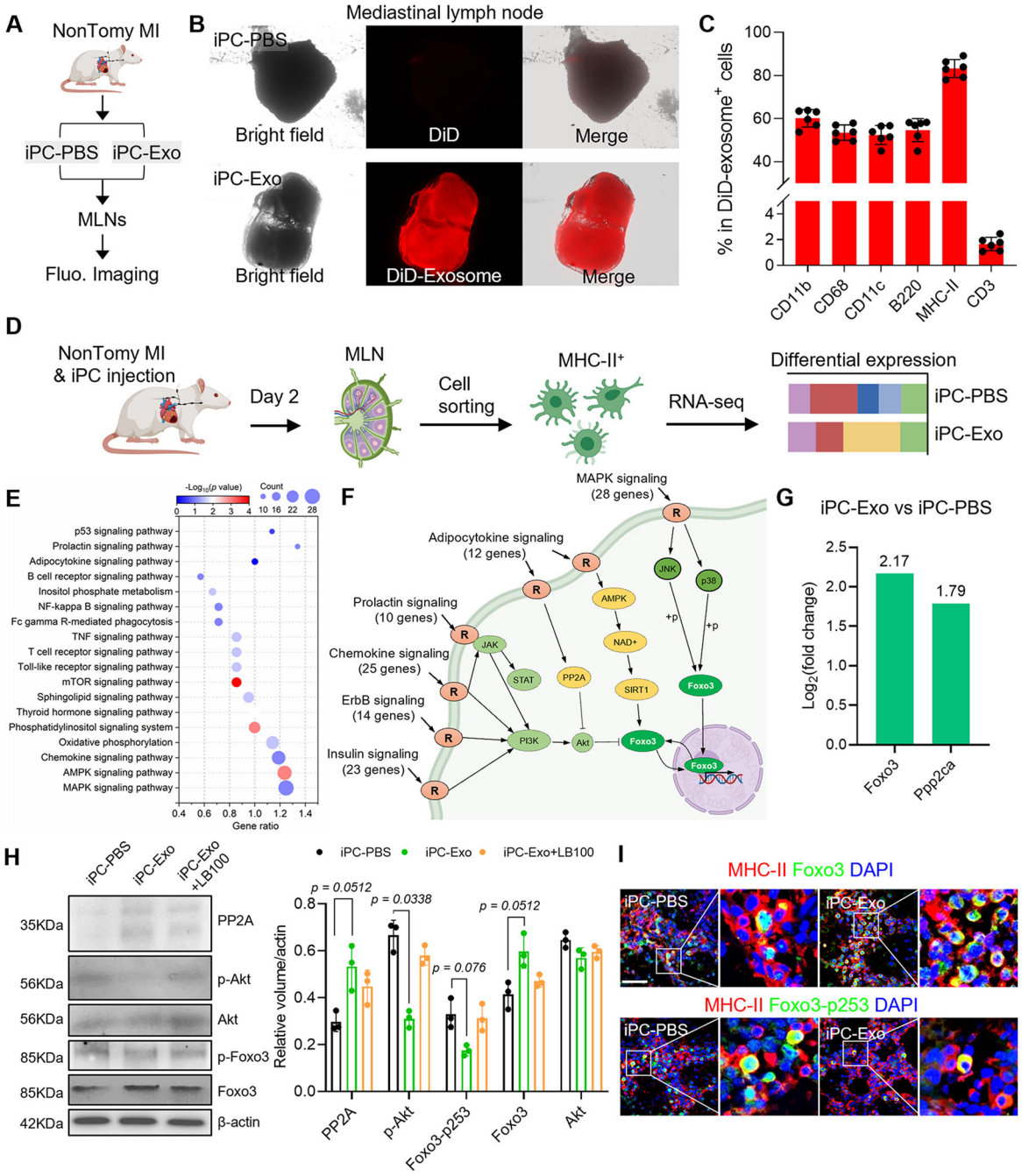

Figure 2. iPC injection of MSC-exosomes promotes Foxo3 activation in APCs.

(**A**) Schematic illustration of intrapericardial injection of MSC-exosomes for MI treatment. (**B**) Macroscopic fluorescent imaging to show the accumulation of MSC-exosomes in the MLN. (**C**) Flowcytometric detection of exosomes uptake by cells in the MLN. n=6 animals for each test. (**D**) Study design for RNA-seq analysis. (**E**) KEGG pathway enrichment analysis. (**F**) Integrated analysis of the enriched signal pathways. (**G**) Analysis of Foxo3 and PP2A(Ppp2ca) expression in RNA-seq data. The values were shown as relative expression compared to iPC-PBS group. (**H**) Western-blot detection of PP2A, p-Akt, Foxo3 and

Foxo3-p253 in APCs. Quantitative data was acquired from three independent tests. (**I**) Immunostaining detection of Foxo3 and Foxo3-p253 expression in the MLN. Scale bar, 60μm. Quantitative data was shown as mean ± SD. *p* value was determined by Kruskal-Wallis's test with Dunn's correction for H.

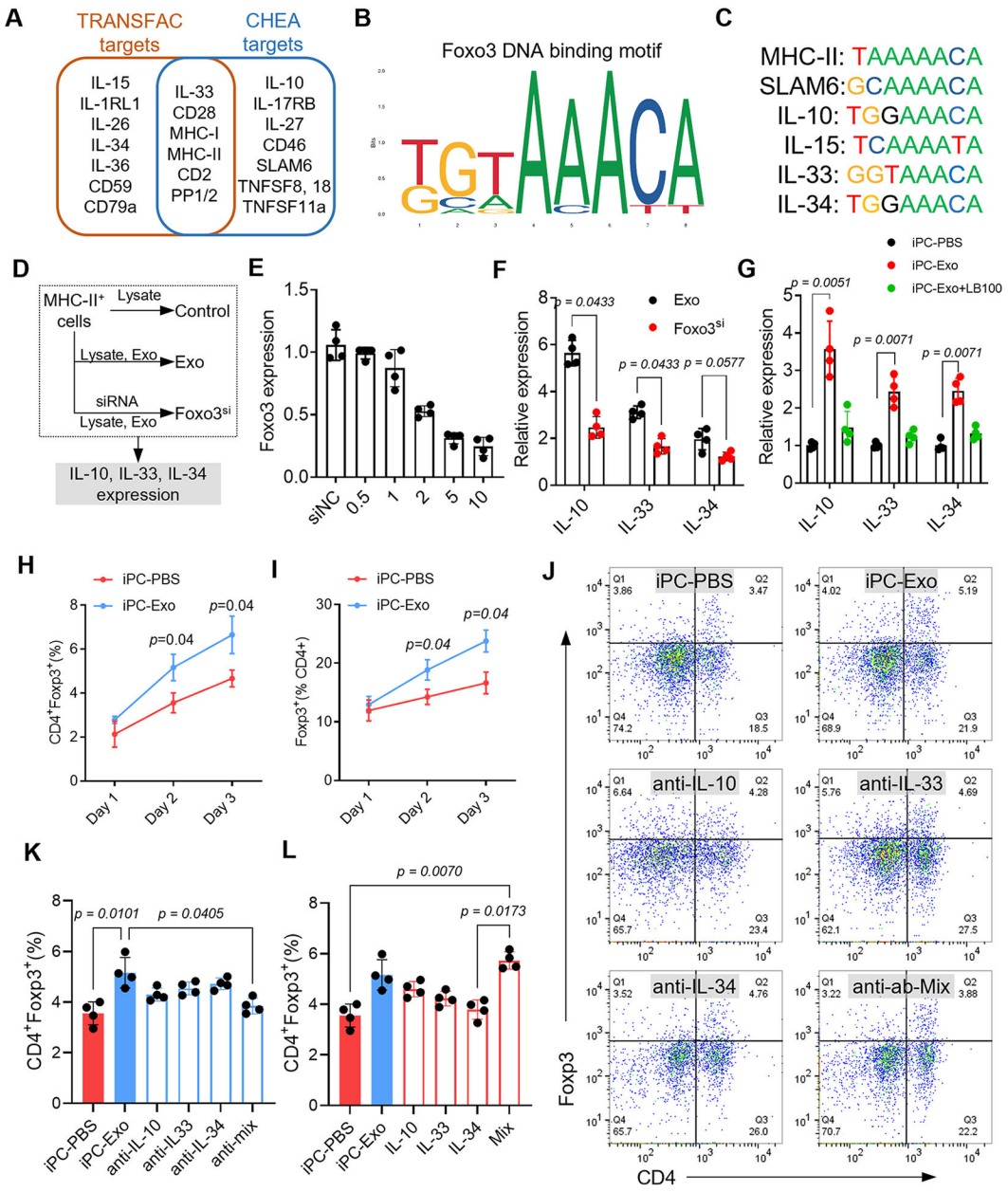

Fig. 3. Foxo3 dominates Treg differentiation by inducing IL-10, IL-33, and IL-34 expression.

(A) Foxo3 downstream target gene prediction. (B) The DNA binding motif of Foxo3. (C) The potent binding sequence of Foxo3 in the promoter sequence of the indicated genes. (D) *In vitro* study design to investigate the functions of Foxo3 in IL-10, IL-33 and IL-34 expression. (E) Investigation of effective siRNA concentration for Foxo3 knockdown. n=4 repeats for each concentration. (F) qRT-PCR detection of indicated cytokines expression. n=4 repeats for each detection. The values were shown as relative expression compared to the mean of control group. (G) qRT-PCR detection of indicated cytokines expression in sorted MHC-II$^+$ cells. n=4 animals for each detection. The values were shown as relative expression compared to iPC-PBS group. (H-I) Quantitative data of flow cytometry detection of CD4$^+$Foxp3$^+$ Tregs in the MLN at indicated time points. n=4 animals for each time point.

(J) Flow cytometry detection of $CD4^+Foxp3^+$ Tregs in the mediastinal lymph node. (K) Quantitative data of flowcytometry indicating that intrapericardial injection of neutralizing antibody or the mix (anti-Mix) abolished iPC-Exo induced Tregs elevation. n=4 animals for each test. (L) Quantitative data of flowcytometry indicating that intrapericardial injection of cytokines (IL-10, IL-33, IL-34 or the Mix) promoted Tregs generation in iPC-PBS treated rats. n=4 animals for each test. Quantitative data was shown as mean ± SD. *p* value was determined by nonparametric Mann-Whitney test for F, H, I (multiple comparisons); and Kruskal-Wallis's test with Dunn's correction for G, K, L.

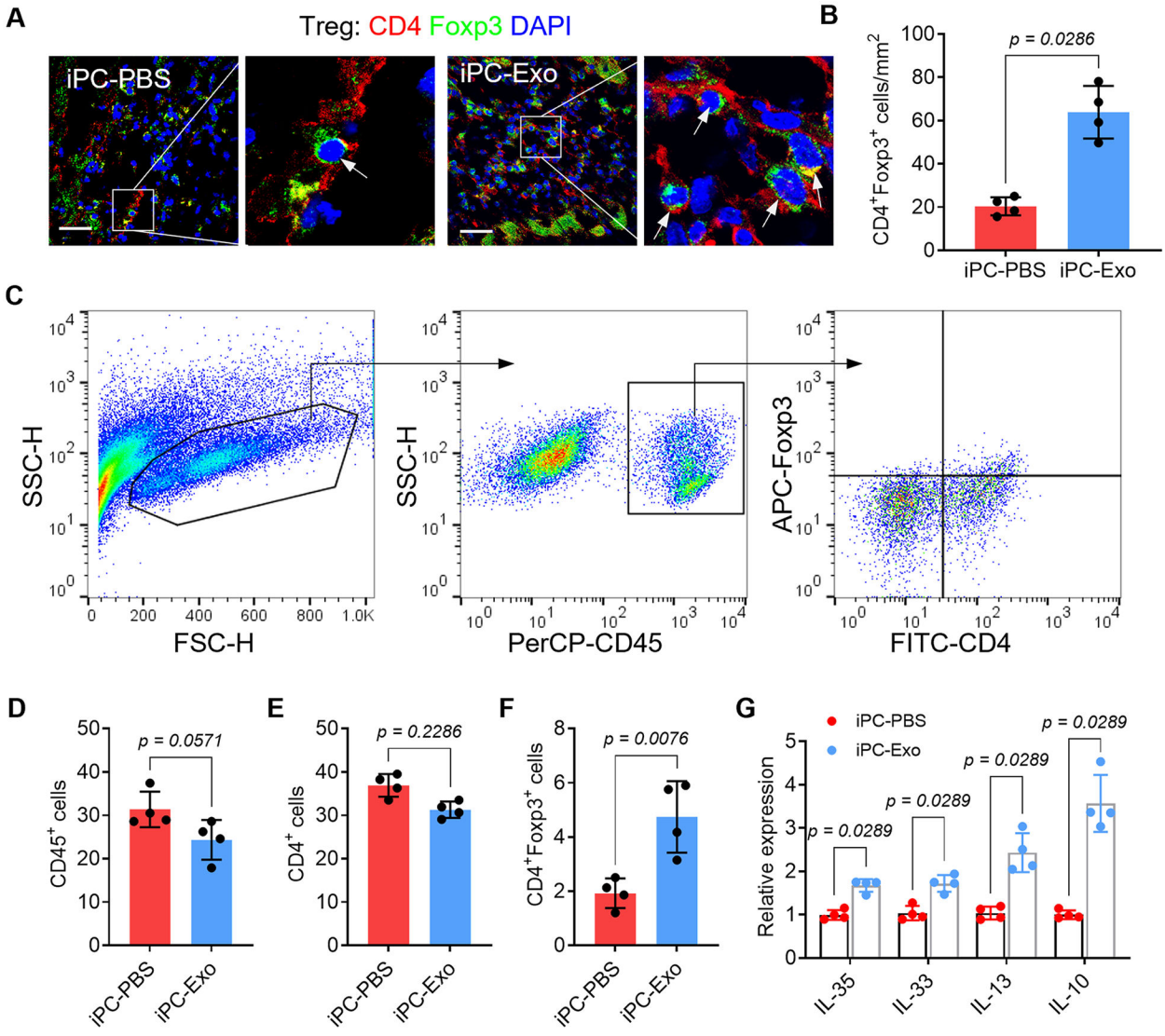

Fig. 4. Intrapericardial injection of exosomes promoted cardiac deployment of Treg cells.

(A) Immunofluorescent detection of Treg distribution in the infarct. Scale bar, 60μm. (B) Quantitative data of Treg infiltration in the infarct. n=4 animals for each group. (C) Gate strategy for detecting Tregs in the infarct by flowcytometry. (D-F) Quantitative data of the indicated cells in the infarct. (G) qRT-PCR detection of Treg-associated cytokines expression in the heart. The values were shown as relative expression compared to iPC-PBS group. Quantitative data were shown as mean ± SD, n=4 animals for each group. *p* value was determined by unpaired 2-tailed nonparametric Mann-Whitney test for B, D-F and G (multiple comparisons).

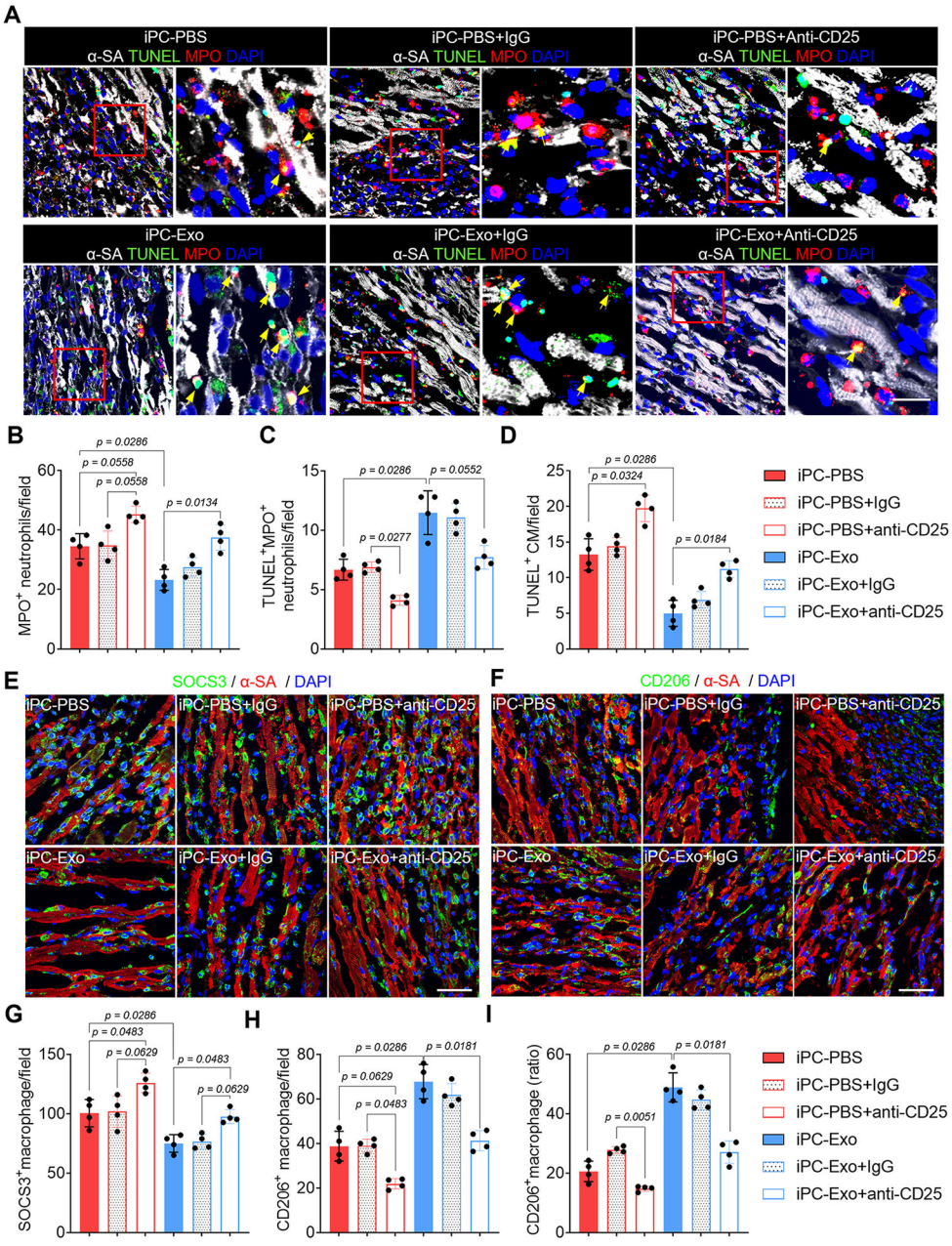

Figure 5. Tregs orchestrate cardiac inflammation resolution.

(A) Detection of neutrophils apoptosis by TUNEL assay. Scale bar, 60μm. (B-C) Quantitative analysis of neutrophils apoptosis. (D) Detection of cardiomyocyte apoptosis by TUNEL assay. (E-I) Detection of macrophage polarization, and accordingly, the counts of $SOCS3^+$ and $CD206^+$ macrophages as well as the $CD206^+$ macrophage ratio in the total macrophages was calculated (I). Scale bar, 60μm. Quantitative data was shown as mean ± SD, n=4 animals for each group. *p* value was determined by Kruskal-Wallis's test with Dunn's correction and nonparametric Mann-Whitney test (iPC-PBS v.s. iPC-Exo) for B-D, G-I.

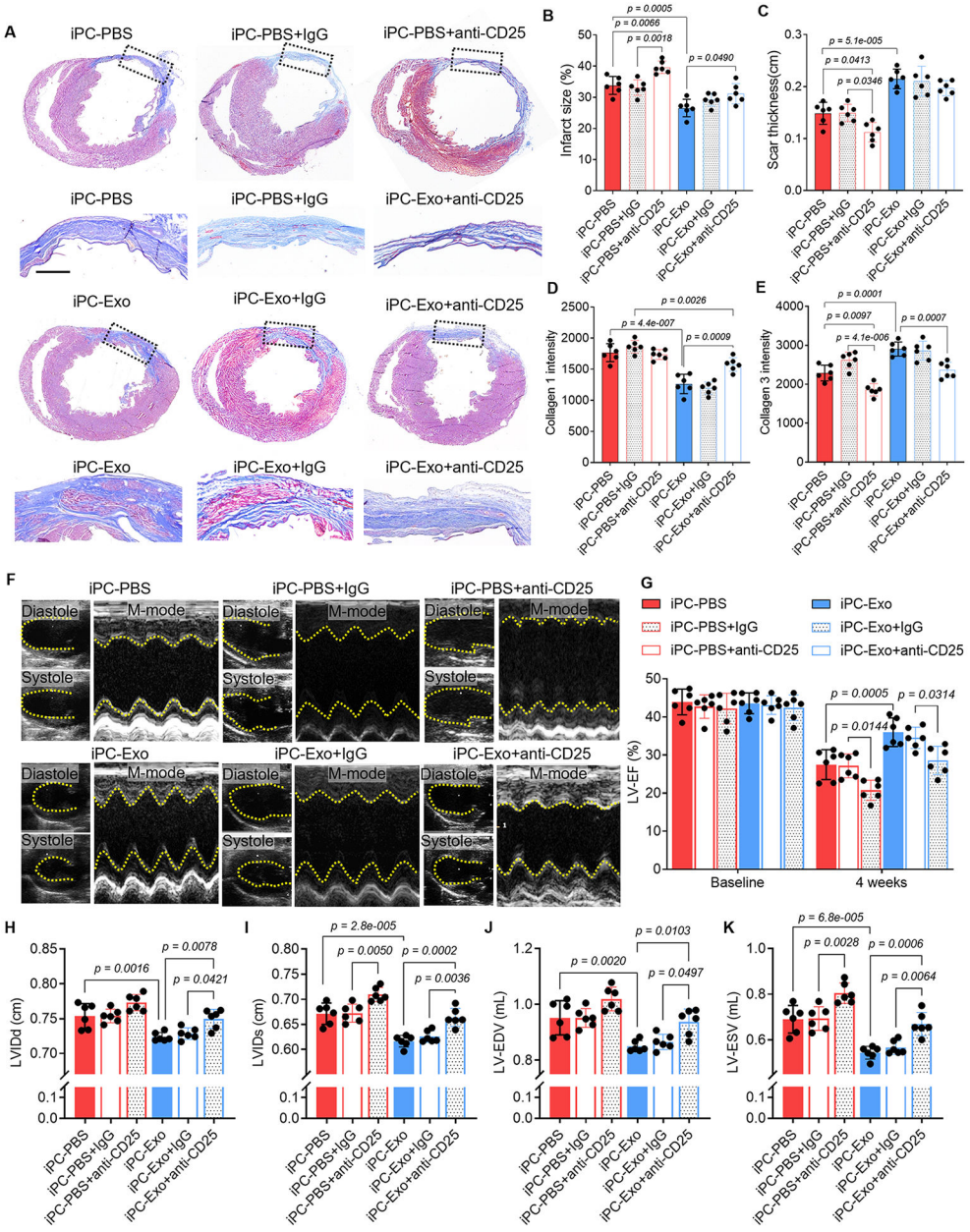

Figure 6. iPC injection of MSC-exosomes promotes cardiac repair.

(A) Masson's trichrome staining to show the histological improvement of the infarct after intrapericardial exosomes treatment. Scale bar, 1mm. (B-C) Quantitative data of infarct size (B) and the scar thickness(C). (D-E) Quantitative data showing the deposition of collage 1 and collagen 3 in the infarct scar from Picrosirius red stained sections. (F) Echocardiography measurement of cardiac function. (G) Quantitative analysis of LV-EF. (H-K) Quantitative analysis of LV dimensions, internal diameters as well as endo volume at both systole and diastole (LVIDd, LVIDs, LV-EDV and LV-ESV). Quantitative data was shown as mean ± SD, n=6 animals for each group. *p* value was determined by two-way ANOVA with Tukey's correction for B-E, G-K.

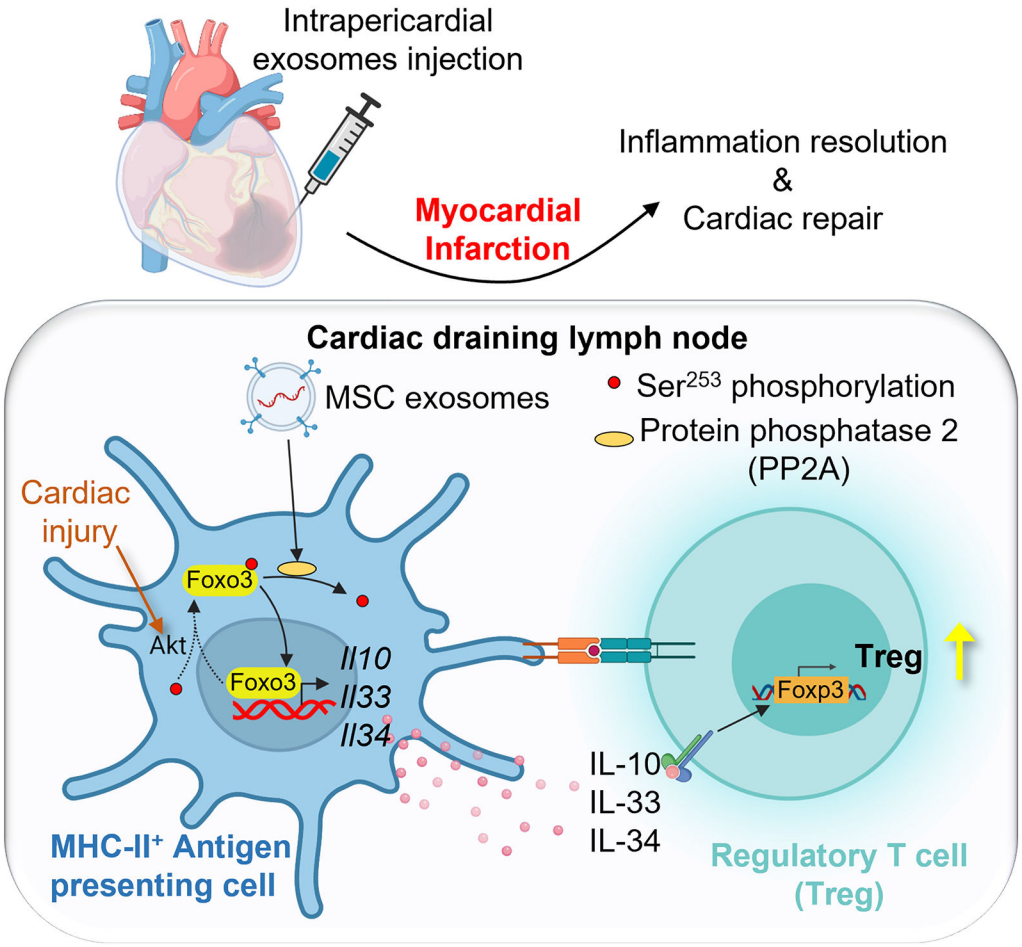

Figure 7. Schematic illustration of the mechanisms underlying the immunomodulating effects of MSC-exosomes to induce Tregs for heart repair.

Uptake of exosomes induced Foxo3 activation via modulating PP2A/p-Akt/Foxo3 pathway. Foxo3 promoted expression and secretion of IL-10, IL-33, IL-34 by MHC-II^{+} APCs to establish a Treg-inducing niche in the MLN. Following myocardial deployment, Tregs orchestrate inflammation resolution and cardiac reparation.